

Tunneling properties versus electronic structures in Si/SiO₂/Si junctions from first principlesEunjung Ko,^{1,*} Kwang-Ryeol Lee,² and Hyoung Joon Choi^{3,†}¹*College of Applied Science, Kyung Hee University, Yongin 446-701, Republic of Korea*²*Center for Computational Science, Institute for Multidisciplinary Convergence of Matter, KIST, Seoul 136-791, Republic of Korea*³*Department of Physics and IPAP, Yonsei University, Seoul 120-749, Republic of Korea*

(Received 27 March 2012; revised manuscript received 3 July 2012; published 29 July 2013)

Using first-principles calculations, we study tunneling properties and electronic structures of Si(001)/SiO₂/Si(001) junctions in a wide energy range covering the local energy gap in the SiO₂ regions. We show that the tunneling spectra $T(E)$ as functions of energy E have overall similarity to the projected densities of states (PDOS) at the centers of the SiO₂ regions, but $T(E)$ and PDOS have significant difference in their dependencies on the SiO₂ thickness. From the energy dependencies of $T(E)$ and PDOS, distinctive energy ranges are recognized in the valence and conduction bands, reflecting the local electronic structures in the SiO₂ region induced from the Si regions. From the difference in the SiO₂-thickness dependencies of $T(E)$ and PDOS and from eigenchannel analysis, we find that the tunneling wave function inside the SiO₂ region decreases with a decay rate which itself decreases as the tunneling distance increases, resulting in a smaller averaged decay rate per length for a thicker SiO₂ region. These results provide a rich picture for the SiO₂ barrier in the aspects of tunneling and local electronic structures, and a theoretical framework generally applicable to other tunneling barriers.

DOI: [10.1103/PhysRevB.88.035318](https://doi.org/10.1103/PhysRevB.88.035318)

PACS number(s): 73.40.Gk, 71.15.Mb, 73.40.Ty, 85.30.De

I. INTRODUCTION

For Si-based nanometer-scale electronic devices, many experimental and theoretical studies have been performed on Si/SiO₂ interfaces and Si/SiO₂/Si structures.^{1–39} Various experimental methods have been employed to find atomic and electronic structures of Si/SiO₂ interfaces, including x-ray photoelectron spectroscopy,^{1,2} electron energy loss spectroscopy,³ core-level spectroscopy,^{4,5} high-resolution medium-energy ion scattering,⁶ and Si 2*p* photoemission spectroscopy (PES).^{7–10} It is found experimentally that suboxidized Si layers (SiO_{*x*}) are present at Si/SiO₂ interfaces, showing all oxidation states.^{1–5,7,8} Regarding the current blocking role of SiO₂ layers, tunneling currents have been measured by scanning tunneling microscopy of Si/SiO₂ structures^{11,12} and by direct current-voltage measurements of Si/SiO₂/Si devices.^{13–15}

Theoretical studies have been performed on atomic structures, electronic properties, and tunneling properties of Si/SiO₂ interfaces and Si/SiO₂/Si structures.^{16–36} Atomic structures of Si/SiO₂ interfaces in Si/SiO₂/Si structures have been modeled by using crystalline SiO₂ structures,^{16–20} first-principles molecular dynamics,^{21,22} and the Monte Carlo approach.^{23,24} Electronic properties of Si/SiO₂ interfaces have been examined in Si/SiO₂/Si structures^{25–28} and Si/SiO₂ superlattices.²⁹ Tunneling properties through nanometer-thick SiO₂ layers in Si/SiO₂/Si structures have been studied with a semiempirical tight-binding scattering method³⁰ and first-principles methods.^{31–36} In particular, effects of defects on the tunneling current were studied with the matrix Green's function method,³⁴ and effects of interfacial structures on the tunneling current were investigated with the real-space finite-difference approach³⁵ and the scattering-state method.³⁶

One of the final goals of the above studies is to establish quantitative dependence of the transport properties on the atomic structures. This can be achieved by understanding the relationships between the transport properties and the

electronic structures as well as between the electronic structures and the atomic structures. In the cases of nanostructures with insulating SiO₂ regions, it is appropriate to compare the tunneling spectrum through SiO₂ regions and the density of states (DOS) inside the SiO₂ regions. In principle, the former is a non-equilibrium property requiring an open boundary condition, while the latter is an equilibrium property that can be obtained with a periodic boundary condition. In the literature, Demkov *et al.*³³ compared the overall energy dependencies of the tunneling spectra and the local density of states (LDOS), and Kang *et al.*³⁴ performed detailed comparison of the tunneling spectra and LDOS to find defect-assisted electron tunneling. Here, in our present work, we compare detailed energy dependencies of the tunneling spectra in Si/SiO₂/Si junctions and the projected densities of states (PDOS) onto atoms near or inside the SiO₂ regions, with and without orbital decomposition, in order to clarify the tunneling properties depending on the atomic structures of the junctions.

In Si/SiO₂/Si junctions, tunneling properties through SiO₂ regions can be understood in terms of Si-induced midgap states in SiO₂ regions, which are evanescent waves that connect smoothly to propagating states in the Si regions. In bulk SiO₂, evanescent waves are energy eigenstates with complex wave vectors, whose imaginary parts provide decay rates of the wave functions through SiO₂ regions. Previous theoretical studies have investigated tunneling through SiO₂ insulators by considering the smallest decay rate corresponding to the smallest imaginary part of the complex wave vectors.^{30,32,37} This is the case when a SiO₂ region is thick enough for the tunneling to be dominated by the slowest decaying state, but other decaying states may also contribute to the tunneling for an ultrathin SiO₂ case. In our present work, we clarify decaying behaviors of midgap states inside ultrathin SiO₂ regions by comparing SiO₂-thickness dependencies of tunneling spectra and PDOS and by analyzing the wave functions for eigenchannels.

In this paper, we present first-principles calculations of tunneling properties through ultrathin SiO₂ regions in Si(001)/SiO₂/Si(001) junctions and compare them with electronic structures inside and near the SiO₂ regions. We show that tunneling spectra $T(E)$ and PDOS at centers of the SiO₂ regions have overall similarity in their energy dependencies, but have significant difference in their dependencies on the SiO₂ thickness. From their energy dependencies, we distinguish three energy ranges in the valence and conduction bands, respectively: (i) low energy ranges within 1 ~ 2 eV from the Si band edges, (ii) intermediate energy ranges beyond 1 ~ 2 eV but within 3 eV, and (iii) high energy ranges beyond 3 eV. These distinctive energy ranges reflect electronic structures in the SiO₂ region induced from the Si regions. We also analyze the difference in the SiO₂-thickness dependencies of $T(E)$ and PDOS, and perform eigenchannel analysis. With these, we show that the decay rate per length of a tunneling wave function is not independent of the tunneling distance inside the SiO₂ region, but it decreases slightly as the tunneling distance increases, which results in a smaller averaged decay rate per length for a thicker SiO₂ case. Similar features should exist in other semiconductor/insulator/semiconductor (SIS) junctions, so our results provide a general guide for inferring tunneling properties of SIS junctions from their atomic and electronic structures.

II. CALCULATION METHODS AND ATOMIC STRUCTURES

Our present work is based on the first-principles density functional method for electronic structures as implemented in the SIESTA code⁴⁰ and the first-principles scattering-state method for electronic transport as implemented in the SCARLET code.⁴¹ The local density approximation (LDA) is used for the exchange-correlation energy and *ab initio* norm-conserving pseudopotentials^{42,43} are used for electron-ion interactions. Electronic wave functions are expanded with pseudoatomic orbitals (double ζ polarization).¹⁹ The electron density is obtained by integrating the wave functions with a $4 \times 4 \times 4$ k grid in the full Brillouin zone of a supercell containing a Si/SiO₂/Si junction. Real-space grids are generated with a cutoff energy of 200 Ry to represent the electron density distribution and the LDA exchange-correlation potential in the real space. Since the wave functions are represented as linear combinations of pseudoatomic orbitals, it is straightforward to calculate PDOS onto atomic sites, with and without orbital decomposition, by using the coefficients of the linear combinations.

As mentioned in the introduction, the tunneling spectrum $T(E)$ and PDOS are different properties in the sense that $T(E)$ is a nonequilibrium property requiring an open boundary condition while PDOS is an equilibrium property that can be obtained with a periodic boundary condition. Thus, while PDOS can be obtained with ordinary methods for electronic structures using a supercell containing a Si/SiO₂/Si junction, the calculation of $T(E)$ needs a special method that can handle a Si/SiO₂/Si junction with no periodic boundary condition along the normal direction to the Si/SiO₂ interfaces; i.e., both of the Si regions in the junction are regarded thick infinitely along the normal direction.

Tunneling spectra $T(E)$ through SiO₂ regions are obtained by using the first-principles scattering-state method⁴¹ with a 12×12 k_{\parallel} grid in the two-dimensional Brillouin zone perpendicular to the tunneling direction. The wave vectors k_{\parallel} are associated with the supercell lattice vectors parallel to Si/SiO₂ interfaces. For a given Si/SiO₂/Si junction, the tunneling spectrum $T(E)$ is obtained in three steps. First, using the self-consistent Hamiltonian of the Si/SiO₂/Si junction and that of bulk Si, we calculate the scattering-state wave function $\psi_{n,E,k_{\parallel}}$ for the incident state of the n th band of the bulk Si having the energy E and the parallel wave vector k_{\parallel} . Details of the scattering-state method are described in Ref. 41. Then we estimate the tunneling probability $T_n(E, k_{\parallel})$ from $\psi_{n,E,k_{\parallel}}$ and calculate the sum $T(E, k_{\parallel})$ of $T_n(E, k_{\parallel})$ over the bands for each E and k_{\parallel} ; i.e., $T(E, k_{\parallel}) = \sum_n T_n(E, k_{\parallel})$. Finally, we average $T(E, k_{\parallel})$ over k_{\parallel} to obtain the tunneling spectrum $T(E)$. Since the number of bands is proportional to the cross-sectional area A of the supercell parallel to the Si/SiO₂ interfaces, the spectrum $T(E)$ is proportional to the area A when a sufficient number of k_{\parallel} are used for the average. In our present work, the area A is 0.7679×0.7679 nm². For the eigenchannel analysis, we obtain the tunneling eigenchannels by diagonalizing the transmission matrix, $t^{\dagger}t$.⁴⁴

We note that if the tunneling probability $T_n(E, k_{\parallel})$ is close to 1 for more than one band at an energy E and a parallel wave vector k_{\parallel} , the spectrum $T(E, k_{\parallel})$ can be larger than 1 because it is defined as the sum of $T_n(E, k_{\parallel})$ for all bands having the energy E and the wave vector k_{\parallel} . In addition, if $T(E, k_{\parallel})$ is larger than 1 at enough fraction of the two-dimensional Brillouin zone, the k_{\parallel} -averaged spectrum $T(E)$ can also be larger than 1. Although one may redefine the spectrum $T(E)$ so that it cannot be larger than 1, e.g., by dividing it by the number of bands, our present definition for $T(E)$ is suitable for transport properties because it is proportional to the conductance at infinitesimal bias voltage.

To construct simple atomic models of Si/SiO₂/Si structures, we use the known β -cristobalite SiO₂ structure and place it between two Si (001) surfaces, matching a surface unit cell of the SiO₂ (001) surface with $\sqrt{2} \times \sqrt{2}$ times the surface unit cell of the Si (001) surfaces. According to the PES experiment, the three suboxide transition layers are present at each Si/SiO₂ interface: The first layer consists of Si¹⁺ and Si²⁺ while Si³⁺ and Si⁴⁺ are distributed over the second and third layers from the interface.⁷ When we place a β -cristobalite SiO₂ region between the two Si (001) surfaces, we rearrange oxygen atoms at each Si/SiO₂ interface to eliminate dangling bonds and produce suboxide transition layers. Similar to the PES experimental results, our model structures have two suboxide transition layers at each Si/SiO₂ interface,^{16,36} as shown in Fig. 1. The first interfacial layer has equal number of Si¹⁺ and Si²⁺ and the second interfacial layer has Si³⁺ only.

Detailed atomic structures are obtained by relaxing the atomic positions until all residual forces are smaller than 0.09 eV/Å with the $4 \times 4 \times 4$ k grid. During the relaxation, the lattice constant c of the supercell perpendicular to the interfaces is relaxed while the lattice constants a and b parallel to the interfaces are fixed to 0.7679 nm. Figure 1 shows relaxed atomic structures of Si(001)/SiO₂/Si(001) junctions with four different SiO₂ thicknesses: 0.54, 0.64, 1.34, and 2.04 nm. Here,

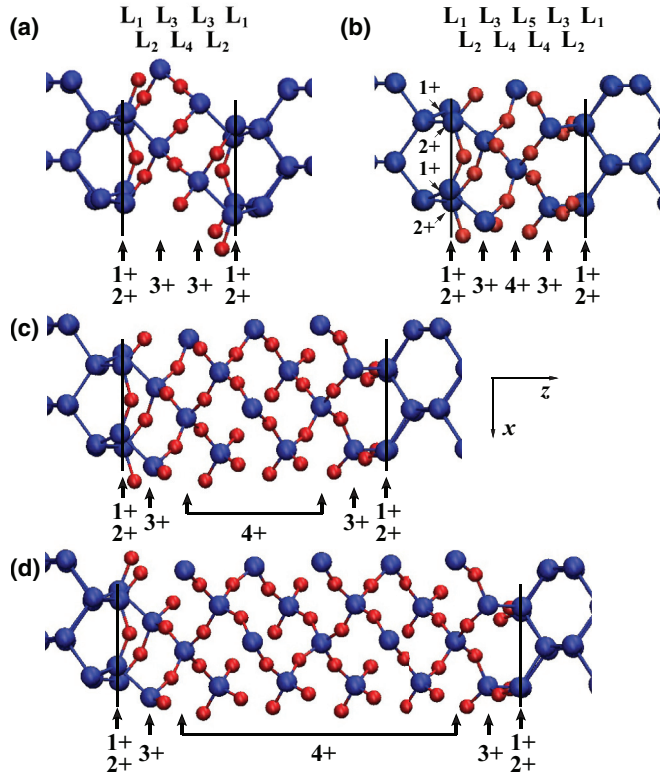


FIG. 1. (Color online) Atomic structures of Si/SiO₂/Si structures with suboxide transition layers: (a) $d_{\text{SiO}_2} = 0.54$ nm, (b) $d_{\text{SiO}_2} = 0.64$ nm, (c) $d_{\text{SiO}_2} = 1.34$ nm, and (d) $d_{\text{SiO}_2} = 2.04$ nm. Large (blue) and small (red) dots are Si and O atoms, respectively. The marks 1+, 2+, 3+, and 4+ denote Si¹⁺, Si²⁺, Si³⁺, and Si⁴⁺ ions, respectively. Vertical solid lines denote averaged Si positions on Si (001) surfaces, with which we measure d_{SiO_2} . In (c), the x and z axes are drawn. In (a) and (b), L_1 , L_3 , and L_5 indicate Si layers and L_2 and L_4 indicate O layers. Atomic structures are repeated periodically along the x and y directions. For PDOS calculation, atomic structures are also repeated along the z direction with large periodicity. For tunneling calculation, atomic structures are not repeated along the z direction; instead, two Si regions are infinitely thick in either the $+z$ or $-z$ direction, sandwiching a SiO₂ region only once.

we define the SiO₂ thickness (d_{SiO_2}) as the distance between averaged Si positions on Si (001) surfaces.

As shown in Fig. 1(a), the 0.54-nm thick SiO₂ region is so thin that the region has only Si¹⁺, Si²⁺, and Si³⁺ ions without any Si⁴⁺ ion surrounded by four oxygen atoms. Compared with the 0.54-nm case, the 0.64-nm thick SiO₂ region has one more O layer and one Si⁴⁺ layer, which are marked as L_4 and L_5 layers, respectively, in Fig. 1(b). The 1.34-nm thick SiO₂ region has four more layers of Si and O, corresponding to one more unit cell of β -cristobalite SiO₂, than the 0.64-nm thick one, and the 2.04-nm thick SiO₂ region has four more layers of Si and O than the 1.34-nm thick one. The addition of the four layers of Si and O atoms results in a 0.7-nm increase of SiO₂ thickness in optimized atomic structures. This is consistent with the lattice constant c of the bulk β -cristobalite SiO₂, which is relaxed to 0.7191 nm when the lattice constants a and b are fixed to 0.7679 nm. The number of Si⁴⁺ layers, which are important for the barrier height, is 0, 1, 5, and 9

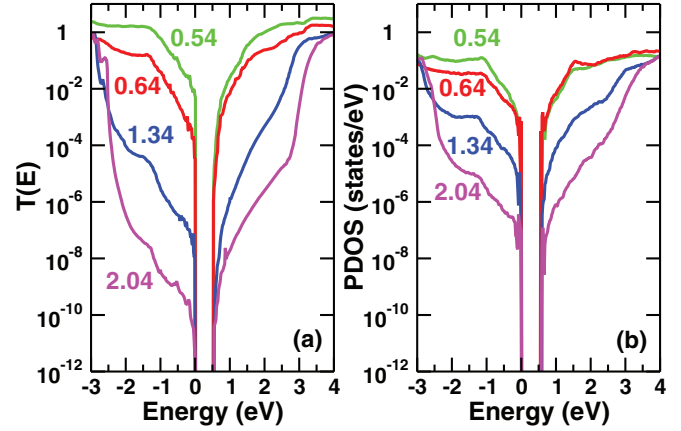


FIG. 2. (Color online) Tunneling spectra $T(E)$ and PDOS in Si/SiO₂/Si junctions. (a) Tunneling spectra $T(E)$ as functions of the energy E . (b) PDOS at an atom at the center of each SiO₂ region. The central atom is O in the 0.54-nm case and it is Si in the other cases. In (a) and (b), the valence band maximum is set to be zero and the SiO₂ thicknesses, 0.54, 0.64, 1.34, and 2.04 nm, are given inside the plots. In (a), values of $T(E)$ are larger than one at some energy ranges because $T(E)$ in our work is defined as the sum of the tunneling probabilities of all bands at the energy E , as described in Sec. II, and the tunneling probability is close to one for more than one band at the energy ranges.

inside the 0.54, 0.64, 1.34, and 2.04-nm thick SiO₂ regions, respectively.

III. TUNNELING SPECTRA VERSUS PROJECTED DENSITIES OF STATES

Figure 2 shows calculated tunneling spectra $T(E)$ in the Si/SiO₂/Si junctions and PDOS at an atom at the center of the SiO₂ regions. The central atom is oxygen in the 0.54-nm thick SiO₂ case and silicon in the other cases, and PDOS at Si atoms only will be considered for the thickness dependence of PDOS. In Fig. 2, both $T(E)$ and PDOS are zero from 0 eV to 0.54 eV, which is due to the energy gap of 0.54 eV in Si regions. Our LDA method underestimates the experimental band gap of 1.12 eV in bulk Si, and it is a well-known limitation of LDA methods. As shown in Fig. 2, plots of $T(E)$ look similar to those of PDOS. We will first discuss similarity in the energy dependencies of $T(E)$ and PDOS, and then discuss difference in their SiO₂-thickness dependencies.

From the energy dependencies of $T(E)$ and PDOS, we distinguish three energy ranges in the valence band: (i) a low energy range within 1.2 eV from the Si valence band maximum (VBM), i.e., $-1.2 \text{ eV} < E < 0.0 \text{ eV}$, (ii) an intermediate energy range beyond the low energy range but within 3.0 eV from the Si VBM, i.e., $-3.0 \text{ eV} < E < -1.2 \text{ eV}$, and (iii) a high energy range beyond the intermediate energy range, i.e., $E < -3.0 \text{ eV}$. For the conduction band, we also distinguish three energy ranges: (i) a low energy range within 1.0 ~ 2.2 eV from the Si conduction band minimum (CBM), i.e., $0.54 \text{ eV} < E < 1.5 \sim 2.7 \text{ eV}$, (ii) an intermediate energy range beyond the low energy range but within 3.0 eV from the Si CBM, i.e., $1.5 \sim 2.7 \text{ eV} < E < 3.5 \text{ eV}$, and (iii) a high energy range beyond the intermediate energy range, i.e., $E > 3.5 \text{ eV}$. Here,

the boundary energy between the low and intermediate energy ranges changes gradually from $E = 1.5$ eV to 2.7 eV as the SiO_2 thickness increases. As E approaches VBM or CBM, $T(E)$ and PDOS decrease most rapidly in the low energy ranges in the 0.54-nm and 0.64-nm thick SiO_2 cases, while they decrease most rapidly in the intermediate energy ranges in the 1.34-nm and 2.04-nm thick SiO_2 cases. We will discuss the origins of the energy dependencies of $T(E)$ and PDOS in Sec. IV, where PDOS are analyzed site-by-site from the Si/SiO₂ interface to the center of the SiO₂ region.

These distinctive energy ranges for $T(E)$ and PDOS were not noticeable in our previous work,³⁶ where $T(E)$ were calculated only at energies very close to the Si band edges, focused on the effects of different interfacial atomic structures on the leakage current. In our present work, we consider $T(E)$ in a wide energy range to characterize tunneling properties of SiO₂ regions up to charge-carrier energies comparable to effective barrier heights of the SiO₂ regions, and compare $T(E)$ with PDOS to understand their energy and thickness dependencies.

In Fig. 2, $T(E)$ and PDOS in the energy range from -3.0 eV to 3.5 eV decrease with the increase of the SiO₂ thickness. Since VBM and CBM in the Si regions are 0.0 eV and 0.54 eV, respectively, the decrease of $T(E)$ and PDOS in the energy range from -3.0 eV to 3.5 eV suggests that effective barrier heights are about 3.0 eV for both the valence and the conduction bands in the Si/SiO₂/Si junction with the SiO₂ thickness of 2.04 nm. In a junction of different semiconductors or a junction of a semiconductor and an insulator, band offsets of valence and conduction bands play the role of effective barrier heights for holes and electrons, respectively. Thus, we need to estimate valence and conduction band offsets.

As shown in Fig. 2(b), PDOS is exactly zero only between 0.0 eV and 0.54 eV at the centers of the SiO₂ regions, so we need to neglect small values of PDOS using a given cutoff criterion to estimate effective local VBM and CBM at the centers of the SiO₂ regions. In our present work, we choose 0.01 states/eV per atom as the cutoff criterion and neglect PDOS smaller than that. Then, the effective local VBM at the centers of the 0.54, 0.64, 1.34, and 2.04-nm SiO₂ regions are $E = -0.48, -0.71, -2.70,$ and -2.56 eV, respectively, and the effective local CBM are $E = 1.14, 1.08, 2.65,$ and 3.11 eV, respectively.⁴⁵ Effective local energy gaps, which are the difference between the effective local VBM and CBM, are 1.62, 1.79, 5.35, and 5.67 eV at the centers of the 0.54, 0.64, 1.34, and 2.04-nm SiO₂ regions, respectively. Since our LDA calculation results in 6.73 eV for the energy gap of bulk SiO₂, the effective local energy gap of 5.67 eV at the center of the 2.04-nm thick SiO₂ region is still about 1 eV smaller than the energy gap of bulk SiO₂.

The effective local VBM, CBM, and energy gaps at the centers of the SiO₂ regions, which are mentioned above, depend on the value of the cutoff criterion of PDOS. If one takes a greater value for the cutoff criterion, one would have a lower effective local VBM and a higher effective local CBM, and thus greater effective barrier heights for the valence and the conduction bands. In the above estimation, we used the cutoff criterion of 0.01 states/eV and obtained $E = -2.56$ eV for the effective local VBM and $E = 3.11$ eV for the effective local CBM at the center of the 2.04-nm thick SiO₂ region.

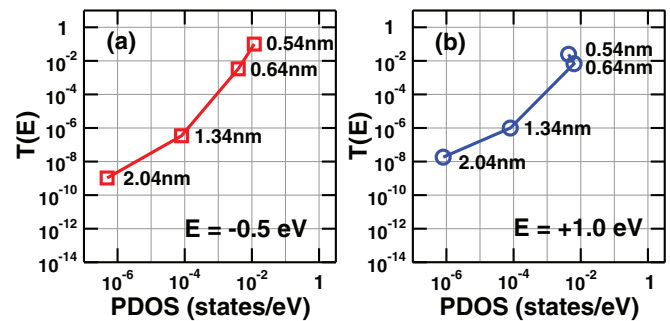


FIG. 3. (Color online) Comparison of tunneling spectra $T(E)$ and PDOS at the center of the SiO₂ region at fixed energies, (a) $E = -0.5$ eV and (b) $E = 1.0$ eV. The SiO₂ thicknesses, 0.54, 0.64, 1.34, and 2.04 nm, are given inside the plots.

These values seem to underestimate barrier heights by ~ 0.4 eV when we consider that $T(E)$ is reduced in the energy range from -3.0 eV to 3.5 eV in the 2.04-nm thick SiO₂ case. This underestimation suggests that the cutoff criterion of PDOS should be increased for better estimation of barrier heights, but if we increase the cutoff criterion, we will have significant PDOS inside the effective local energy gap, which may look contradictory to the concept of the energy gap. Thus, we use the values of the effective local VBM, CBM, and energy gaps estimated above, with a caution that they may underestimate barrier heights slightly.

As shown in Fig. 2(a) and more clearly shown in Fig. 3 for two fixed energies, the ratio of $T(E)$ of the 0.64-nm case to that of 1.34-nm case is substantially larger than the ratio of $T(E)$ of the 1.34-nm case to that of the 2.04-nm case. Unlike this behavior of $T(E)$, the ratio of PDOS at the center of the 0.64-nm thick SiO₂ region to that of the 1.34-nm case is almost equal to the ratio of PDOS of the 1.34-nm case to that of the 2.04-nm case. Considering that both $T(E)$ and PDOS at the central atoms are related to states in SiO₂ regions induced from Si regions, it is rather unexpected that $T(E)$ and PDOS have a difference in their dependencies on the SiO₂ thickness.

To analyze physical implications of the difference in the SiO₂-thickness dependencies of $T(E)$ and PDOS, we consider bisecting the SiO₂ region of a Si/SiO₂/Si junction conceptually by a plane parallel with Si/SiO₂ interfaces at the center of the SiO₂ region. Here we consider bisection, for simplicity, and will consider more division later in this section. With the bisection, we consider averaged decay rates per length in the two sections, κ_1 and κ_2 , respectively, which are defined such that the amplitude of an electronic state incident from a Si region into the SiO₂ region is reduced by a factor of $\exp(-\kappa_1 d_{\text{SiO}_2}/2)$, on average, as the state passes through the first section of the SiO₂ region, and the amplitude of the same electronic state is reduced further by a factor of $\exp(-\kappa_2 d_{\text{SiO}_2}/2)$, on average, as it passes through the other section of the SiO₂ region. The values of κ_1 and κ_2 should vary in energy and also depend on the SiO₂ thickness. With κ_1 and κ_2 , we can express the tunneling probability through the SiO₂ region as $T(E) \sim |\exp[-(\kappa_1 + \kappa_2)(d_{\text{SiO}_2}/2)]|^2$ and PDOS at the center in the SiO₂ region as $\text{PDOS} \sim |\exp(-\kappa_1 d_{\text{SiO}_2}/2)|^2$, roughly. If the averaged decay rates, κ_1 and κ_2 , were dependent only on the local electronic structure inside each section of

the SiO₂ region such as the effective local VBM and CBM, κ_1 would be equal to κ_2 because the electronic structures in the two sections of the SiO₂ region are virtually the same with each other. If κ_1 were equal to κ_2 , $T(E)$ would be simply proportional to the square of PDOS. However, as shown clearly in Fig. 3, $T(E)$ does not decrease as fast as the square of PDOS as the SiO₂ thickness increases from 1.34 nm to 2.04 nm, indicating that $\kappa_1 > \kappa_2$ in the 2.04-nm thick SiO₂ region. This implies that the averaged decay rates are not determined solely by the local electronic structure inside each section of the SiO₂ region, but are also dependent on the tunneling distance from an incident Si/SiO₂ interface as discussed below.

We can rationalize $\kappa_1 > \kappa_2$ as follows. When an electron tunnels through a SiO₂ region, the decaying part of its wave function into a SiO₂ region is a linear combination of evanescent waves of the SiO₂ region, each of which has a different decay rate. In the process of tunneling, evanescent waves that decay fast will decay mostly in the first half of the SiO₂ region while evanescent waves that decay slowly will still remain significant and decay in the second half of the SiO₂ region. Thus, it is straightforward that the averaged decay rate κ_1 in the first half of the SiO₂ region is larger than the averaged decay rate κ_2 in the second half of the SiO₂ region. In short, faster decaying evanescent waves contribute more to κ_1 than κ_2 , so κ_1 is greater than κ_2 . The difference, $\kappa_1 - \kappa_2$, will be more substantial in a thicker SiO₂ region unless the SiO₂ region is so thick that both κ_1 and κ_2 converge to the smallest decay rate of the evanescent waves.

In the above discussion we bisected the SiO₂ region for simplicity. In general, the SiO₂ region can be divided into N regions and we can introduce $\kappa_1, \kappa_2, \dots, \kappa_N$ for the average decay rates per length in the regions, respectively. Then, using the same argument in the above, we can conclude that $\kappa_1 > \kappa_2 > \dots > \kappa_N$. Thus the decay rate per length itself decreases as an electronic state tunnels through the SiO₂ region. This finding should be generally applicable to other SIS, metal/insulator/metal (MIM), or metal/semiconductor/metal (MSM) junctions because it is not based on any quantitative material-specific properties of the Si/SiO₂/Si junctions but simply based on the fact that faster decaying evanescent waves contribute more to the average decay rate per length when the tunneling distance is smaller.

Since the average decay rate per length decreases with the barrier thickness, the plot of the logarithmic value of the leakage current as a function of the thickness would be a concave curve when viewed from above. Thus if one predicts the leakage current through a thinner barrier by extrapolating the leakage current as a simple exponential function of the barrier thickness using some results of thicker barriers, one would underestimate the leakage current through the thinner barrier because the current increases more rapidly than the simple exponential function. Similarly, if one predicts the leakage current through a thicker barrier by extrapolating the leakage current as a simple exponential function of the barrier thickness using some results of thinner barriers, one would again underestimate the leakage current through the thicker barrier because the current does not decrease as fast as the simple exponential function. Thus one should take into account the decrease of the average decay rate with the barrier thickness in order to have a precise extrapolation of the

leakage current for thinner or thicker barriers in any SIS, MIM, or MSM junction.

IV. ELECTRONIC STRUCTURES INSIDE THE SiO₂ REGIONS

To understand the energy dependencies of $T(E)$ and PDOS at the center of the SiO₂ region, PDOS are obtained site-by-site from the interface to the center of the SiO₂ region. In Figs. 4(a) and 4(b), PDOS are shown at atomic sites from the left interface to the center of the 0.54-nm and the 0.64-nm thick SiO₂ regions, respectively. In the figures, PDOS at atomic sites closer to the right interface are not shown because they are the same with those closer to the left interface. As shown in Figs. 4(a) and 4(b), in the energy range from -4 eV to -3 eV, PDOS at O sites, which are labeled with L₂ and L₄, are much larger than PDOS at Si sites inside the SiO₂ regions, which are labeled with L₁ and L₃. This indicates that the effective local VBM states inside the SiO₂ region consist mainly of

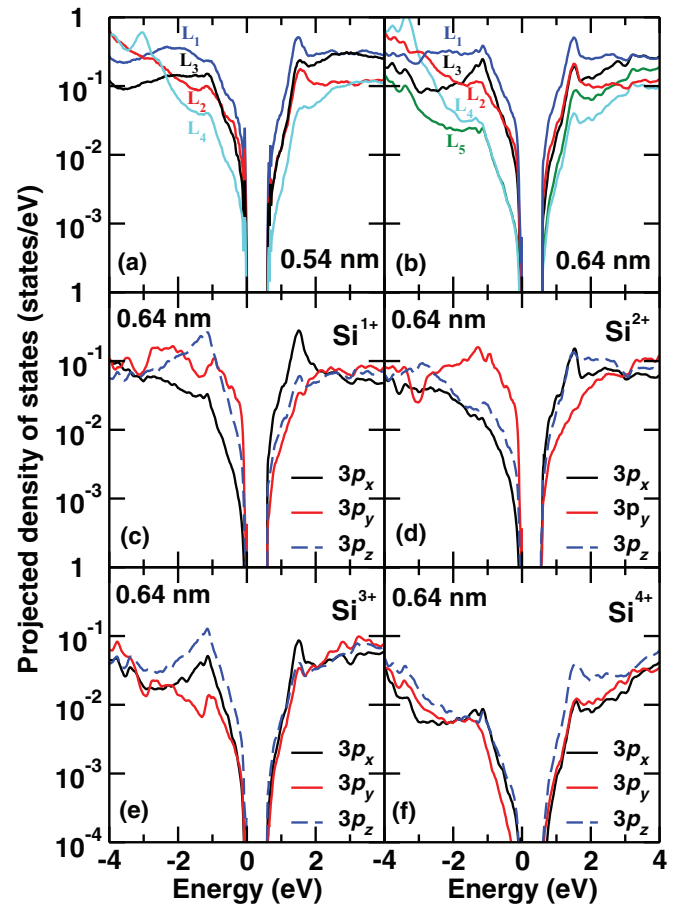


FIG. 4. (Color online) PDOS at atomic sites inside SiO₂ regions. (a) PDOS at the L₁ layer (Si¹⁺ site), the L₂ layer (O site), the L₃ layer (Si³⁺ site), and the L₄ layer (O site) of the 0.54-nm thick SiO₂ region. The L_i layers are marked in Fig. 1(a). (b) PDOS at the L₁ layer (Si¹⁺ site), the L₂ layer (O site), the L₃ layer (Si³⁺ site), the L₄ layer (O site), and the L₅ layer (Si⁴⁺ site) of the 0.64-nm thick SiO₂ region. The L_i layers are marked in Fig. 1(b). (c)–(f) PDOS at the Si¹⁺, Si²⁺, Si³⁺, and Si⁴⁺ sites of the 0.64-nm thick SiO₂ region, respectively. In (c)–(f), black solid, gray (red) solid, and dashed (blue) lines represent $3p_x$, $3p_y$, and $3p_z$ orbital characters of Si, respectively.

oxygen states, which is consistent with the dominant oxygen characters of the states near VBM in bulk β -cristobalite SiO_2 .⁴⁶ In contrast, in the energy range from -2 eV to -1 eV, PDOS at Si sites inside the SiO_2 regions, which are labeled with L_1 and L_3 in Figs. 4(a) and 4(b), are larger than PDOS at O sites, which are labeled with L_2 and L_4 , although the L_3 layer is closer to the center of SiO_2 regions than the L_2 layer is. Similar nonmonotonic decrease of PDOS also occurs in the energy range from 1 eV to 2 eV in the conduction band. These nonmonotonic features in PDOS are accompanied by peaks in PDOS at about -1.2 eV and 1.5 eV.

To find the origin of the peaks in PDOS at about -1.2 eV and 1.5 eV, we obtain orbital decompositions of PDOS at Si^{n+} sites ($n = 1, 2, 3, 4$) inside the 0.64-nm thick SiO_2 region, as shown in Figs. 4(c)–4(f). From the decompositions, we find that the peaks are due to enhancement of specific p orbital characters and they are closely related to the directions of the Si-Si and Si-O bonds. The peaks in PDOS near -1.2 eV in the valence band are due to bonding states of the Si-Si bonds at the suboxide transition layers in the SiO_2 region while the peaks in PDOS near 1.5 eV in the conduction band are due to antibonding states of the Si-Si and Si-O bonds. Especially, two bonds of each Si^{n+} ion, which are directed toward the closer Si/ SiO_2 interface from the Si^{n+} ion, are more important in characterizing the enhanced p orbital characters because neighboring atoms on the side of the closer Si/ SiO_2 interface have much larger PDOS than the other neighboring atoms. This is because electronic states inside the SiO_2 region at the energy near the Si band edges are induced from states in the Si regions, and they decay rapidly toward the center of the SiO_2 region.

In particular, at the Si^{1+} site, which has Si- Si^{1+} bonds on the yz plane, $3p_y$ and $3p_z$ orbital characters are enhanced in PDOS near -1.2 eV, and $3p_x$ orbital character is enhanced in PDOS near 1.5 eV, as shown in Fig. 4(c). At the Si^{2+} site, which has Si- Si^{2+} bonds along the y axis, $3p_y$ orbital character is enhanced in PDOS near -1.2 eV, and $3p_x$ and $3p_z$ orbital characters are enhanced in PDOS near 1.5 eV, as shown in Fig. 4(d). At the Si^{3+} site, which has a Si^{1+} - Si^{3+} bond on the xz plane, $3p_x$ and $3p_z$ orbital characters are enhanced in PDOS near -1.2 eV, and $3p_x$ orbital character is enhanced in PDOS near 1.5 eV, as shown in Fig. 4(e). Here, the orbital character in PDOS near 1.5 eV is affected by the enhanced $3p_x$ orbital character at the neighboring Si^{1+} site at the same energy. Lastly, at the Si^{4+} site, which does not have any neighboring Si^{n+} site ($n = 1, 2, 3, 4$), peak features near -1.2 eV and 1.5 eV are greatly reduced in PDOS, with no specific orbital character except for less reduced Si $3p_z$ orbital character near 1.5 eV, as shown in Fig. 4(f).

When the SiO_2 thickness increases from 0.64 to 1.34 or 2.04 nm, PDOS do not change significantly at atomic sites at and near the Si/ SiO_2 interfaces and decrease gradually toward the center of the SiO_2 region. In particular, the peak in PDOS at $E = -1.2$ eV is gradually reduced at Si^{4+} sites closer to the center of the 1.34- or 2.04-nm thick SiO_2 region, and the peak in PDOS at $E = 1.5$ eV is gradually reduced and shifted to 2.7 eV at Si^{4+} sites toward the center. These features affect the energy dependencies for $T(E)$ and PDOS at the center of the SiO_2 regions, resulting in the distinctive energy ranges described in Sec. III.

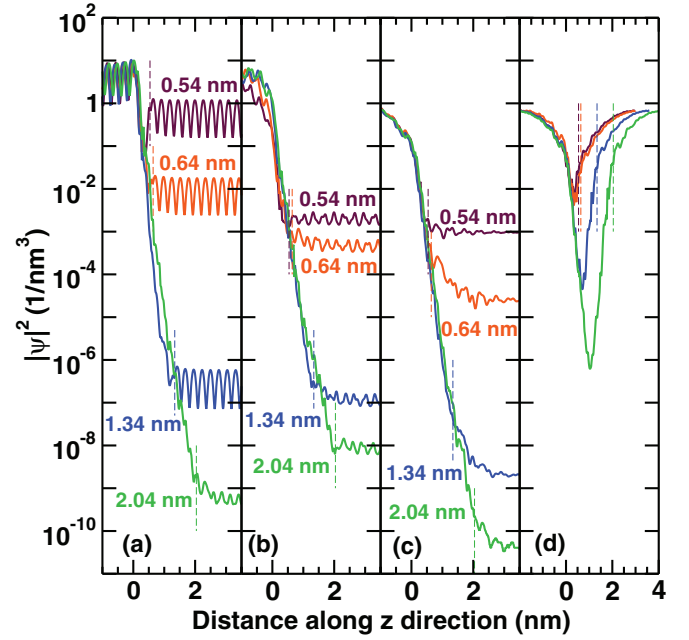


FIG. 5. (Color online) (a)–(c) Squared amplitudes, $|\psi|^2$, of tunneling wave functions of the maximally tunneling eigenchannels in Si/ SiO_2 /Si junctions with different SiO_2 thicknesses (a) at VBM at $(k_x, k_y) = (0, 0)$, (b) at CBM at $(k_x, k_y) = (0, 0)$, and (c) at CBM at $(k_x, k_y) = (\delta, 0)$. Here, δ corresponds to the wave vector at CBM of bulk Si. (d) Squared amplitudes, $|\psi|^2$, of wave functions at CBM at $(k_x, k_y) = (\delta, 0)$, calculated with a Bloch-like periodic boundary condition imposed along the z direction of Si/ SiO_2 /Si junctions. In (d), the SiO_2 thicknesses are 0.54, 0.64, 1.34, and 2.04 nm from top to bottom lines. In (a)–(d), the z direction is perpendicular to Si/ SiO_2 interfaces, and the x and y directions are parallel to the interfaces. In each Si/ SiO_2 /Si junction, two Si/ SiO_2 interfaces are located at $z = 0$ and $z = d_{\text{SiO}_2}$, respectively, which are marked with vertical dotted lines. In (a)–(c), the tunneling eigenchannels are calculated for incident waves from the $z < 0$ region. In (a)–(d), squared amplitudes of the wave functions are averaged in the xy plane at each z position.

V. WAVE FUNCTIONS INSIDE THE SiO_2 REGIONS

We analyze the wave functions inside the SiO_2 regions by calculating wave functions of the maximally tunneling eigenchannels corresponding to the largest eigenvalues of the transmission matrix, $t^{\dagger}t$.⁴⁴ We consider only the maximally tunneling eigenchannels because the other eigenchannels contribute negligibly to $T(E)$ in our present work. Figures 5(a)–5(c) show squared amplitudes of the wave functions of maximally tunneling eigenchannels at VBM at $(k_x, k_y) = (0, 0)$, CBM at $(k_x, k_y) = (0, 0)$, and CBM at $(k_x, k_y) = (\delta, 0)$ in Si/ SiO_2 /Si junctions, respectively. Here, δ corresponds to the wave vector at CBM of bulk Si. Overall, the squared amplitudes of the wave functions of the maximally tunneling eigenchannels decrease gradually inside the SiO_2 regions with a decay rate that depends weakly but nonnegligibly on the tunneling distance. In Sec. III, we compared $T(E)$ and PDOS and showed that the decay rate of the wave functions inside the SiO_2 regions decreases as the tunneling distance increases. In this section, Figs. 5(a)–5(c) show directly that logarithms of the squared amplitudes of the

wave functions inside SiO₂ regions are not in straight lines as functions of the z position, but they have a slight upward curvature, indicating the decrease of the decay rates. Thus, the averaged decay rate, per length, through the SiO₂ region decreases as the SiO₂ thickness increases.

When we compare the transmitted wave functions of the maximally tunneling eigenchannels after the SiO₂ region shown in Figs. 5(b) and 5(c), our results show that the wave function amplitudes are slightly larger for the eigenchannels at CBM at $(k_x, k_y) = (0, 0)$ than those at CBM at $(k_x, k_y) = (\delta, 0)$ for all SiO₂ thicknesses. In addition, except for the 0.54-nm thick SiO₂ case, the tunneling wave functions undergo additional decay inside the transmitted Si regions which are on the right side of vertical dashed lines in Figs. 5(a)–5(c). This additional decay occurs in Si/SiO₂/Si structures where Si-Si bond directions at the right interfaces do not match with those at the left interfaces. In the 0.54-nm case, Si-Si bonds at the left and right interfaces are on the yz plane, as shown in Fig. 1(a), while in the other cases, Si-Si bonds are on the xz plane at the right interface, as shown in Figs. 1(b)–1(d). This suggests possible enhancement of the current-blocking role by making Si-Si bond directions different at the left and the right interfaces.

For comparison, Fig. 5(d) shows squared amplitudes of wave functions at CBM, obtained with the Bloch-like periodic boundary condition along the z direction, which we call “periodic” states. The wave vectors $(k_x, k_y, k_z) = (\delta, 0, k_z)$ of the periodic states are carefully chosen to make the energies of the periodic states equal to the energy at CBM at which we calculated the tunneling states shown in Fig. 5(c). Since only a single eigenchannel exists near CBM at $(k_x, k_y) = (\delta, 0)$, we can choose a single periodic state which satisfies $E(\delta, 0, k_z) = E_c$ for a given energy E_c near CBM. In Fig. 5(d), the periodic states decay from the left and right interfaces into the SiO₂ region with a decay rate almost independent of the SiO₂ thickness. This implies that the considered SiO₂ thicknesses are too small to have significant variation in the decay rate of the periodic states because the decay length for the periodic states is only one half of the SiO₂ thickness, while the decay length for the tunneling states is the whole of the SiO₂ thickness. We also note that, although it is not shown in the figure, orbital characters of the periodic states in the SiO₂ region near the left interface are similar to those of the tunneling states incident from the left interface.

Figure 6 shows squared amplitudes of the tunneling wave functions of the maximally tunneling eigenchannels in the 2.04-nm case. The tunneling wave functions are obtained at valence-band energies $E_{v1} = -0.06$ eV, $E_{v2} = -1.49$ eV, and $E_{v3} = -2.93$ eV, marked in Fig. 6(d), and at conduction-band energies $E_{c1} = 0.54$ eV, $E_{c2} = 1.99$ eV, and $E_{c3} = 3.42$ eV, marked in Figs. 6(e) and 6(f). The squared amplitudes of the wave functions are averaged over the xy plane and plotted along the z direction. To compare wave functions at energies below and above the effective barrier height, the energy E_{v1} is chosen very close to the Si VBM, E_{v3} is lower than the effective local VBM at the center of the SiO₂ region, i.e., beyond the effective barrier height in the valence band, and E_{v2} is the middle of E_{v1} and E_{v3} . Similarly, the energy E_{c1} is chosen very close to the Si CBM, E_{c3} is higher than the effective local CBM at the center of the SiO₂ region, i.e., beyond the effective

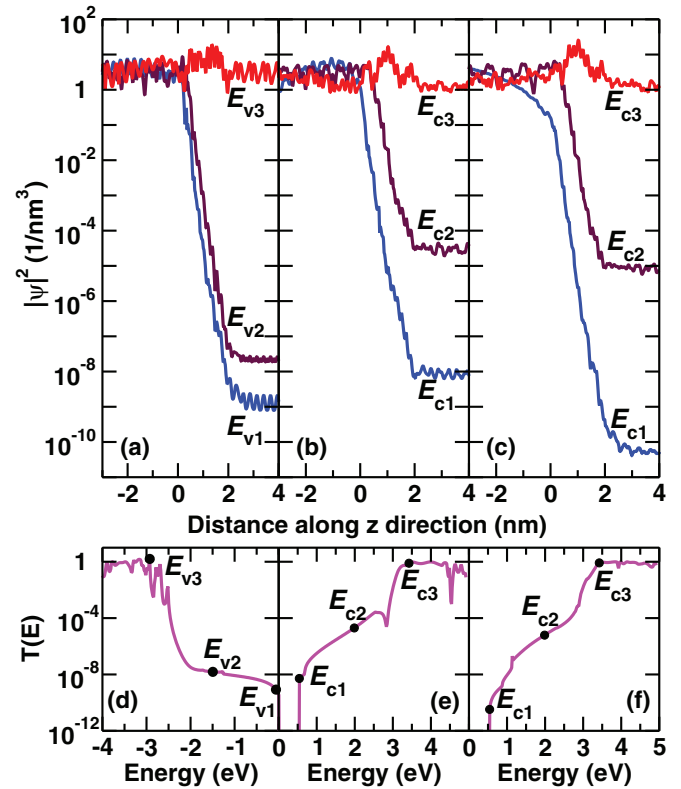


FIG. 6. (Color online) (a)–(c) Squared amplitudes, $|\psi|^2$, of tunneling wave functions of the maximally tunneling eigenchannels at different energies in the Si/SiO₂/Si junction with the 2.04-nm thick SiO₂ region. Wave functions are obtained at valence-band energies, $E_{v1} = -0.06$ eV, $E_{v2} = -1.49$ eV, and $E_{v3} = -2.93$ eV, and conduction-band energies, $E_{c1} = 0.54$ eV, $E_{c2} = 1.99$ eV, and $E_{c3} = 3.42$ eV. The in-plane wave vector is $(k_x, k_y) = (0, 0)$ for the wave functions plotted in (a) and (b), and $(k_x, k_y) = (\delta, 0)$ for those in (c). In (a)–(c), the tunneling eigenchannels are calculated for incident waves from the $z < 0$ region, and the squared amplitudes of the wave functions are averaged in the xy plane at each z position. (d) and (e) Tunneling spectra for $(k_x, k_y) = (0, 0)$. (f) Tunneling spectrum for $(k_x, k_y) = (\delta, 0)$.

barrier height in the conduction band, and E_{c2} is the middle of E_{c1} and E_{c3} .

As shown in Figs. 6(a)–6(c), the decay rates inside the SiO₂ region and the amplitudes of the transmitted parts of the wave functions vary greatly at energies below and above the effective barrier heights. Figure 6(a) shows that the amplitude of the wave function at E_{v1} is greatly reduced in the SiO₂ region while that at E_{v3} does not decay there. Similar features are shown in Figs. 6(b) and 6(c) for the conduction-band states at E_{c1} and E_{c3} . At E_{v2} , the amplitude of the wave function is closer to that at E_{v1} than at E_{v3} , as shown in Fig. 6(a). This is consistent with Fig. 6(d), where the tunneling probability at E_{v2} is closer to that at E_{v1} than at E_{v3} . At E_{c2} , the amplitudes of the wave functions are in the middle, in logarithmic scale, of those at E_{c1} and E_{c3} , as shown in Figs. 6(b) and 6(c). This reflects the exponential increase of the tunneling probability in the energy range from E_{c1} to E_{c3} , as shown in Figs. 6(e) and 6(f). At energies near E_{v3} , the wave functions of the maximally tunneling eigenchannels vary very

rapidly and abruptly as a function of energy (not shown in figures), implying that the electronic structure inside the SiO₂ region is complicated at the energies near the effective local VBM. In contrast, at energies near E_{c3} , the wave functions of the maximally tunneling eigenchannels change very slowly with respect to the energy and show a common pattern in their real-space shapes (not shown in figures), implying a simple band structure in the SiO₂ region at energies near the effective local CBM. As for different valleys in Si CBM, Figs. 6(b) and 6(c) show that the amplitude of the transmitted part of the wave function at E_{c1} is larger for $(k_x, k_y) = (0, 0)$ than for $(k_x, k_y) = (\delta, 0)$. This is consistent with Figs. 6(e) and 6(f), where the tunneling probability near Si CBM, i.e., near E_{c1} , is larger for $(k_x, k_y) = (0, 0)$ than that for $(k_x, k_y) = (\delta, 0)$.

VI. CONCLUSIONS

We presented tunneling properties in Si/SiO₂/Si junctions and compared them with electronic structures in an energy range covering the local energy gap in the SiO₂ regions as functions of the SiO₂ thickness from 0.54 nm to 2.04 nm by first-principles calculations. We showed that $T(E)$ and PDOS at the central atomic site inside the SiO₂ region have overall similarity as functions of energy E , but significant difference in their SiO₂-thickness dependencies. Energy dependencies of $T(E)$ and PDOS are found to change at about 1 eV below VBM of Si regions and at about 1 ~ 2 eV above CBM of Si regions due to electronic states at and near Si/SiO₂ interfaces,

which are shown to originate from the atomic structures at the interfaces. Thus, in general, atomic structures at and near semiconductor/oxide interfaces can produce significant common features shared by the energy dependencies of $T(E)$ through the oxide and PDOS at the center of the oxide. Comparison of $T(E)$ and PDOS and the eigenchannel analysis show that the tunneling wave function decreases inside the SiO₂ region with the decay rate per length which itself decreases slowly as the electron tunnels through the SiO₂ region. This yields a smaller averaged decay rate per length for a thicker SiO₂ region. This finding can be applicable to other barriers, in general, and it is especially important for a precise extrapolation of the leakage current as a function of the barrier thickness. Our results provide detailed information on tunneling and local electronic structures in the SiO₂ barrier and will be useful in studying other oxide barriers.

ACKNOWLEDGMENTS

This work was supported by the Korean Ministry of Education, Science, and Technology (WCU R31-10016), by NRF of Korea (Grant No. 2011-0018306), and by the Converging Research Center Program through the Ministry of Education, Science, and Technology (2012K001314). Computational resources have been provided by Academic Computing Center at Global Campus, Kyung Hee University, and KISTI Supercomputing Center (Project No. KSC-2011-C3-05).

*eunjungko04@gmail.com

†h.j.choi@yonsei.ac.kr

- ¹F. J. Grunthaler, P. J. Grunthaler, R. P. Vasquez, B. F. Lewis, J. Maserjian, and A. Madhukar, *J. Vac. Sci. Technol.* **16**, 1443 (1979).
- ²A. Ishizaka and S. Iwata, *Appl. Phys. Lett.* **36**, 71 (1980).
- ³D. A. Muller, T. Sorsch, S. Moccio, F. H. Baumann, K. Evans-Lutterodt, and G. Timp, *Nature (London)* **399**, 758 (1999).
- ⁴G. Hollinger and F. J. Himpsel, *Appl. Phys. Lett.* **44**, 93 (1984).
- ⁵F. J. Himpsel, F. R. McFeely, A. Taleb-Ibrahimi, J. A. Yarmoff, and G. Hollinger, *Phys. Rev. B* **38**, 6084 (1988).
- ⁶H. C. Lu, T. Gustafsson, E. P. Gusev, and E. Garfunkel, *Appl. Phys. Lett.* **67**, 1742 (1995).
- ⁷J. H. Oh, H. W. Yeom, Y. Hagimoto, K. Ono, M. Oshima, N. Hirashita, M. Nywa, A. Toriumi, and A. Kakizaki, *Phys. Rev. B* **63**, 205310 (2001).
- ⁸K. Ohishi and T. Hattori, *Jpn. J. Appl. Phys.* **33**, L675 (1994).
- ⁹J. W. Keister, J. E. Rowe, J. J. Kolodziej, H. Niimi, T. E. Madey, and G. Lucovsky, *J. Vac. Sci. Technol. B* **17**, 1831 (1999).
- ¹⁰M. M. Banaszak Holl and F. R. McFeely, *Phys. Rev. Lett.* **71**, 2441 (1993).
- ¹¹M. Tabe and M. Tanimoto, *Appl. Phys. Lett.* **58**, 2105 (1991).
- ¹²P. Sutter, W. Ernst, and E. Sutter, *Appl. Phys. Lett.* **85**, 3148 (2004).
- ¹³H. S. Momose, M. Ono, T. Yoshitomi, T. Ohguro, S. Nakamura, M. Saito, and H. Iwai, *IEEE Trans. Electron Devices* **43**, 1233 (1996).
- ¹⁴N. Yang, W. K. Henson, J. R. Hauser, and J. J. Wortman, *IEEE Trans. Electron Devices* **46**, 1464 (1999).

- ¹⁵S. Uno, A. Ishida, K. Deguchi, Y. Kamakura, and K. Taniguchi, *J. Appl. Phys.* **89**, 8336 (2001).
- ¹⁶I. Ohdomari, H. Akatsu, Y. Yamakoshi, and K. Kishimoto, *J. Non-Cryst. Solids* **89**, 239 (1987); *J. Appl. Phys.* **62**, 3751 (1987).
- ¹⁷M. Hane, Y. Miyamoto, and A. Oshiyama, *Phys. Rev. B* **41**, 12637 (1990).
- ¹⁸A. Pasquarello, M. S. Hybertsen, and R. Car, *Phys. Rev. Lett.* **74**, 1024 (1995); *Appl. Phys. Lett.* **68**, 625 (1996); *Appl. Surf. Sci.* **104**, 317 (1996); *Phys. Rev. B* **53**, 10942 (1996).
- ¹⁹A. Korkin, J. C. Greer, G. Bersuker, V. V. Karasiev, and R. J. Bartlett, *Phys. Rev. B* **73**, 165312 (2006).
- ²⁰H. Kageshima and K. Shiraishi, *Phys. Rev. Lett.* **81**, 5936 (1998).
- ²¹A. Pasquarello, M. S. Hybertsen, and R. Car, *Nature (London)* **396**, 58 (1998).
- ²²A. A. Demkov and O. F. Sankey, *Phys. Rev. Lett.* **83**, 2038 (1999).
- ²³Y. Tu and J. Tersoff, *Phys. Rev. Lett.* **84**, 4393 (2000).
- ²⁴K.-O. Ng and D. Vanderbilt, *Phys. Rev. B* **59**, 10132 (1999).
- ²⁵J. B. Neaton, D. A. Muller, and N. W. Ashcroft, *Phys. Rev. Lett.* **85**, 1298 (2000).
- ²⁶A. Stirling, A. Pasquarello, J.-C. Charlier, and R. Car, *Phys. Rev. Lett.* **85**, 2773 (2000).
- ²⁷B. R. Tuttle, *Phys. Rev. B* **67**, 155324 (2003).
- ²⁸M. Watarai, J. Nakamura, and A. Natori, *Phys. Rev. B* **69**, 035312 (2004).
- ²⁹N. Tit and M. W. C. Dharma-Wardana, *Solid State Commun.* **106**, 121 (1998); *J. Appl. Phys.* **86**, 387 (1999).
- ³⁰M. Städele, B. R. Tuttle, and K. Hess, *J. Appl. Phys.* **89**, 348 (2001).

- ³¹A. A. Demkov, R. Liu, X. Zhang, and H. Loechelt, *J. Vac. Sci. Technol. B* **18**, 2388 (2000).
- ³²X.-G. Zhang, Z.-Y. Lu, and S. T. Pantelides, *Appl. Phys. Lett.* **89**, 32112 (2006).
- ³³A. A. Demkov, X. Zhang, and D. A. Drabold, *Phys. Rev. B* **64**, 125306 (2001).
- ³⁴J. Kang, Y.-H. Kim, J. Bang, and K. J. Chang, *Phys. Rev. B* **77**, 195321 (2008).
- ³⁵T. Ono, *Phys. Rev. B* **79**, 195326 (2009).
- ³⁶E. Ko, K. R. Lee, and H. J. Choi, *Phys. Rev. B* **84**, 033303 (2011).
- ³⁷A. Sakai, A. Ishida, S. Uno, and Y. Kamakura, *J. Comput. Electron.* **1**, 195 (2002).
- ³⁸Khairurrijal, W. Mizubayashi, S. Miyazaki, and M. Hirose, *Appl. Phys. Lett.* **77**, 3580 (2000).
- ³⁹S. Tang, R. M. Wallace, A. Seabaugh, and D. King-Smith, *Appl. Surf. Sci.* **135**, 137 (1998).
- ⁴⁰D. Sánchez-Portal, P. Ordejón, E. Artacho, and J. M. Soler, *Int. J. Quantum Chem.* **65**, 453 (1997).
- ⁴¹H. J. Choi, M. L. Cohen, and S. G. Louie, *Phys. Rev. B* **76**, 155420 (2007).
- ⁴²M. L. Cohen, *Phys. Scr. T* **1**, 5 (1982).
- ⁴³N. Troullier and J. L. Martins, *Phys. Rev. B* **43**, 1993 (1991).
- ⁴⁴M. Brandbyge, M. R. Sørensen, and K. W. Jacobsen, *Phys. Rev. B* **56**, 14956 (1997).
- ⁴⁵The effective local VBM and CBM for the 2.04-nm case given in Ref. 36 are slightly different from our present results because Ref. 36 used PDOS at an oxygen atom near the center of the SiO₂ region to determine the effective local band edges while our present work uses PDOS at the Si atom at the center of the SiO₂ region. Using PDOS at the O or Si site can change estimates of the effective local VBM and CBM near the center of the SiO₂ region by ~0.1 eV and ~0.01 eV, respectively, which are not significant because we use the effective local VBM and CBM for qualitative discussions only.
- ⁴⁶P. M. Schneider and W. B. Fowler, *Phys. Rev. Lett.* **36**, 425 (1976).